

# Highly perturbed molecular gas in infalling cluster galaxies: the case of CGCG97-079

T. C. Scott<sup>1,2\*</sup>, A. Usero<sup>3</sup>, E. Brinks<sup>2</sup>, H. Bravo–Alfaro<sup>4</sup>, L. Cortese<sup>5</sup>, and A. Boselli<sup>6</sup>,  
and M. Argudo–Fernández<sup>7,8,9</sup>

<sup>1</sup>*Institute of Astrophysics and Space Sciences (IA), Rua das Estrelas, 4150-762 Porto, Portugal*

<sup>2</sup>*Centre for Astrophysics Research, University of Hertfordshire, College Lane, Hatfield, AL10 9AB, UK*

<sup>3</sup>*Observatorio Astronómico Nacional, C/Alfonso XII 3, 28014 Madrid, Spain*

<sup>4</sup>*Departamento de Astronomía, Universidad de Guanajuato, Apdo. Postal 144, Guanajuato 36000, Mexico*

<sup>5</sup>*Centre for Astrophysics and Supercomputing, Swinburne University of Technology, PO Box 218 Hawthorn, Victoria 3122, Australia*

<sup>6</sup>*Aix Marseille Université, CNRS, LAM (Laboratoire d’Astrophysique de Marseille) UMR 7326, 13388, Marseille, France*

<sup>7</sup>*Instituto de Astrofísica de Andalucía (CSIC), Apartado 3004, 18080 Granada, Spain*

<sup>8</sup>*Departamento de Física Teórica y del Cosmos, Universidad de Granada, 18071 Granada, Spain*

<sup>9</sup>*Key Laboratory for Research in Galaxies and Cosmology, Shanghai Astronomical Observatory, Chinese Academy of Sciences, 80 Nandan Road, Shanghai, China, 200030*

Accepted

## ABSTRACT

We report on CO ( $J = 2 \rightarrow 1$ ) mapping with the IRAM 30-m HERA receiver array of CGCG 97-079, an irregular galaxy in the merging galaxy cluster Abell 1367 ( $z = 0.022$ ). We find that  $\sim 80\%$  of the detected CO ( $J = 2 \rightarrow 1$ ) is projected within a 16 arcsec<sup>2</sup> (6.5 kpc<sup>2</sup>) region to the north and west of the optical/NIR centre, with the intensity maximum offset  $\sim 10$  arcsec (4 kpc) NW of the optical/NIR centre and  $\sim 7$  arcsec (3 kpc) south-east of the HI intensity maximum. Evolutionary synthesis models indicate CGCG 97-079 experienced a burst of star formation  $\sim 10^8$  yr ago, most likely triggered by a tidal interaction with CGCG 97-073. For CGCG 97-079 we deduce an infall velocity to the cluster of  $\sim 1000$  km s<sup>-1</sup> and moderate ram pressure ( $P_{\text{ram}} \approx 10^{-11}$  dyn cm<sup>-2</sup>). The observed offset in CGCG 97-079 of the highest density HI and CO ( $J = 2 \rightarrow 1$ ) from the stellar components has not previously been observed in galaxies currently undergoing ram pressure stripping, although previous detailed studies of gas morphology and kinematics during ram pressure stripping were restricted to significantly more massive galaxies with deeper gravitational potential wells. We conclude the observed cold gas density maxima offsets are most likely the result of ram pressure and/or the high-speed tidal interaction with CGCG 97-073. However ram pressure stripping is likely to be playing a major role in the perturbation of lower density gas.

**Key words:** galaxies: CO — galaxies: ISM — galaxies:clusters:individual: (Abell 1367, CGCG 97-079)

## 1 INTRODUCTION

The consensus view is that, in low-redshift galaxy clusters, ram pressure stripping by the intra-cluster medium (ICM) is the dominant mechanism accelerating the evolution of late-type galaxies (van Gorkom 2004; Boselli & Gavazzi 2014; Chung et al. 2009). Models for cluster spirals subject to ram pressure stripping (e.g., Roediger & Hensler 2005; Roediger & Brüggén 2007; Kapferer et al. 2009; Tonnesen & Bryan 2009) indicate that removal of the inter-

stellar medium (ISM) proceeds progressively during a spiral’s infall to the cluster. Initially only the loosely bound peripheral interstellar medium (ISM), principally HI, is stripped. The higher column density HI and molecular gas located in the deepest parts of a galaxy’s potential well, traced by the optical/Near Infrared (NIR) intensity maxima, remain unperturbed until late in the stripping process and requires high velocities relative to the ISM/ICM ( $V_{\text{rel}}$ ) and high ICM densities encountered during a galaxy’s traverse of a cluster core in order to remove them (e.g., Roediger & Hensler 2005; Roediger & Brüggén 2007). The truncated H $\alpha$  and dust disks observed in HI deficient spi-

\* E-mail: tom.scott@astro.up.pt (TCS)

rals are consistent with this picture of outside-in ISM removal (Koopmann & Kenney 2004; Cortese et al. 2010). H I and CO observations and modelling of the Virgo spirals NGC 4522 and NGC 4330 by Vollmer et al. (2008, 2012) are examples showing that during ram pressure stripping the high column density H I and molecular gas remain located deep within the gravitational well traced by the NIR and optically most luminous part of the galaxies. Moreover NGC 4848 (Vollmer et al. 2001) in Coma ( $L_X = 7.8 \times 10^{44}$  ergs  $s^{-1}$ ; Plionis et al. 2009) indicates that even in X-ray luminous clusters a spiral's transit of the cluster core may remove H I without causing a molecular gas deficiency<sup>1</sup>, although the recent work by Boselli et al. (2014) for a sample of Virgo galaxies shows a correlation between molecular and H I deficiencies (see also Fumagalli et al. 2009). The ISM content, morphology and kinematic signatures resulting from extreme ram pressure ( $\sim 10^{-10}$  dyne  $cm^{-2}$ ), as is proposed for ESO 137-001 projected  $\sim 280$  kpc from the center of the Norma cluster ( $M_{dyn} \sim 1 \times 10^{15} M_\odot$ ) from modelling with  $V_{rel} \sim 3000$  km  $s^{-1}$  by Jáchym et al. (2014), are less well studied. Those authors argue extreme ram pressure stripping has already removed all detectable H I from the disk of ESO 137-001 and is now in the process of stripping the molecular gas, as well as being partially responsible for a molecular tail containing approximately half of the galaxy's observed molecular gas. Jáchym et al. (2014) note the stripped H I is likely to have been converted to other phases, including the observed molecular and X-ray tail emission. Even ESO 137-001 appears to have followed the sequential removal of increasingly dense ISM from the galactic disk during ram pressure stripping, with stripping of the molecular disk being delayed until the final stages which are now being witnessed.

There have been relatively few detailed studies of changes in H I and CO morphology and gas kinematics during ram pressure stripping in gas-rich late-type spirals and in particular of dwarf irregular galaxies. Although a Virgo Irr dwarf, IC 3418, with about twice the stellar mass of the SMC, contains evidence of having lost almost all its H I and molecular gas by ram pressure stripping within the last few  $\times 10^8$  yr (Kenney et al. 2014). A sample of late-type dwarf galaxies near the centres of clusters, which are presumed to have lost their H I by ram pressure stripping, display truncated H $\alpha$  disks (Fossati et al. 2013). Also we see clear evidence of truncated UV star-forming disks in both spiral and dwarf galaxies in the Virgo cluster (Cortese et al. 2012). These studies imply dwarfs are subject to the same sequential outside-in gas stripping as higher mass late-type galaxies (Boselli & Gavazzi 2014), a proposition which is supported by the detection of CO in the disk of IC 3418.

The scenario depicted above is challenged by our recent studies of late-type galaxies in the spiral-rich merging cluster Abell 1367 ( $L_X = 1.25 \times 10^{44}$  ergs  $s^{-1}$ ; Plionis et al. 2009) which has a  $M_{dyn} \sim 6.9 \times 10^{14} M_\odot$  (Boselli & Gavazzi 2006), about half that of Coma or Norma, and hosts two sub-clusters in the early stages of an approximately equal mass merger (Donnelly et al. 1998). In Scott et al. (2010, here-

after Paper I), we found an unusually high frequency of offsets between the H I and optical intensity maxima in a sample of the cluster's late-type galaxies. Our multi-pointing CO ( $J = 1 \rightarrow 0$ ) and CO ( $J = 2 \rightarrow 1$ ) observations with the IRAM<sup>2</sup> 30-m telescope (Scott et al. 2013, hereafter Paper II), provided indications of perturbed molecular disks and molecular gas excesses in a subset of the Paper I sample. Together, these papers raise the question whether a mechanism other than standard ram pressure stripping is driving the evolution of spiral galaxies in A 1367, and in merging clusters in general.

CGCG 97-079 is an optically-irregular galaxy with  $D_{25} = 45$  arcsec (18.6 kpc), an estimated  $M_* \sim 1.2 \times 10^9 M_\odot$ , (i.e., of order of the Large Magellanic Cloud or M33) and is projected 420 kpc to the NW of the NW sub-cluster core of A 1367 (Figure 1 in Paper II). That figure also shows the X-ray emission (*ROSAT*) from the A 1367 ICM. Its 50–100 kpc ionised gas and radio continuum tails oriented away from the cluster centre (Figure 1), provide evidence that CGCG 97-079 is undergoing ram pressure stripping (Gavazzi & Jaffe 1987; Gavazzi et al. 2001; Boselli & Gavazzi 2014). However our previous observations (Papers I and II) suggest its neutral (atomic and molecular) gas distributions are inconsistent with current ram pressure stripping models. In particular its molecular and atomic gas intensity maxima lie  $\sim 6$  kpc and  $\sim 12$  kpc, respectively, to the NW from its optical intensity maximum as derived from sparsely sampled CO maps and low resolution H I data. CGCG 97-079 is the clearest case in A 1367 of H I and CO intensity maxima offsets, in apparent contradiction to ram pressure models, making it an interesting target for the investigation of mechanisms driving the the evolution of ISM in galaxies in A 1367.

This paper reports on follow-up CO ( $J = 2 \rightarrow 1$ ) mapping of CGCG 97-079 with the IRAM 30-m HERA receiver array. We also utilised H I C-array data from the NRAO<sup>3</sup> VLA archive (project AG264), a *Spitzer* IRAC<sup>4</sup> 4.5  $\mu m$  image (ID: AORKEY25789696 taken from the Infrared Science Archive IRSA), a *GALEX* FUV image (A1367\_SPEC\_A-fd-int.fits) retrieved from the MAST archive<sup>5</sup>, and an H $\alpha$  image from GOLDMine<sup>6</sup>

Section 2 gives details of the HERA observations, with observational results in section 3. A discussion follows in section 4 with concluding remarks in section 5. Based on a redshift to A 1367 of 0.022 and assuming  $\Omega_m = 0.3$ ,  $\Omega_\Lambda = 0.7$ , and  $H_o = 72$  km  $s^{-1}$  Mpc<sup>-1</sup> (Spergel et al. 2007) the distance to the cluster is 92 Mpc and the angular scale is 1 arcmin  $\sim 24.8$  kpc. All equatorial positions referred to throughout this paper are in J2000.0. References to the optical centre are to the position  $11^h 43^m 13^s.4$ ,  $+20^\circ 00' 17''$  from the NASA/IPAC Extragalactic Database (NED).

<sup>2</sup> Institut de radioastronomie millimétrique (IRAM) is supported by CNRS/INSU (France), the MPG (Germany) and the IGN (Spain).

<sup>3</sup> The National Radio Astronomy Observatory is a facility of the National Science Foundation operated under cooperative agreement by Associated Universities, Inc.

<sup>4</sup> InfraRed Array Camera.

<sup>5</sup> Mikulski Archive for Space Telescopes.

<sup>6</sup> Galaxy Online Database Milano Network, (Gavazzi et al. 2003, <http://goldmine.mib.infn.it/>).

<sup>1</sup> A spiral's H<sub>2</sub> or H I deficiency is defined as the log of the ratio of the expected to observed gas mass. Negative values indicate an excess.

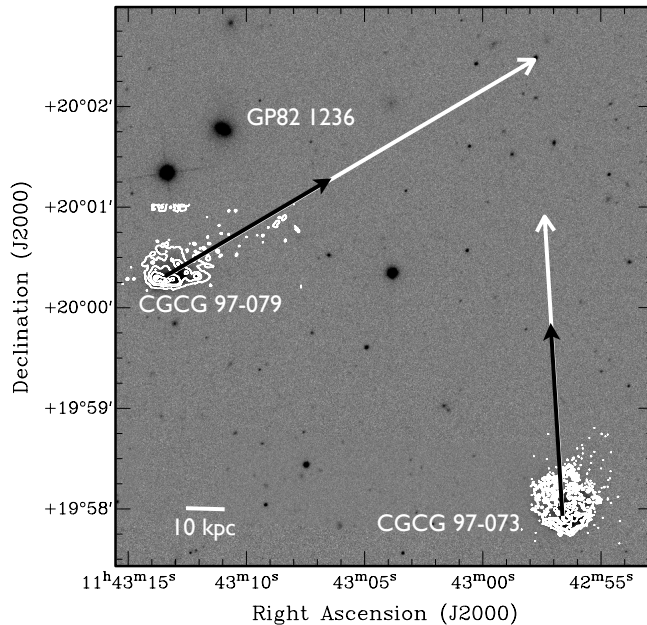


**Figure 1.** CGCG 97-079: SDSS  $r$ -band image with the black (shorter) and white (longer) arrows indicating, respectively, the approximate extent and orientation of the radio continuum (Gavazzi & Jaffe 1987) and  $H\alpha$  tails of CGCG 97-073 and CGCG 97-079. The white arrow head of the CGCG 97-079 tail marks the approximate position where the  $H\alpha$  tails from deep imaging from Boselli & Gavazzi (2014) appear to meet.  $H\alpha$  contours (white) are from a GOLDMine image. The position of the nearest neighbouring galaxy, A 1367 GP82 1236 is also marked.

## 2 OBSERVATIONS–HERA CO MAPPING

$^{12}\text{CO}$  ( $J = 2 \rightarrow 1$ ) emission line mapping of CGCG 97-079 was carried out with the HERA  $3 \times 3$  multi-beam receiver array on the IRAM 30-m telescope at Pico Veleta, Spain, in slightly under sampled dual polarisation “On the Fly” mode with position switching. Receivers used were HERA 1 and 2 with WILMA 1 and 2 backends (1024 channels with 2 MHz separation). Further observational parameters are given in Table 1. The total integration time was 13 hr which was accumulated in March 2010 and January 2012. CO ( $J = 2 \rightarrow 1$ ) was mapped in a  $\sim 1.1 \times 1.1$  arcmin<sup>2</sup> region of sky centred at (-10.6, +10.6 arcsec) from the galaxy’s optical centre. After every three scans ( $\sim 15$  minutes) a chopper wheel calibration was carried out. Pointing was checked at between 1 and 2 hour intervals using the broadband continuum of 3C273.

Data reduction was carried out using GILDAS software and excluded spectra taken under particularly poor conditions. Spectra were then summed position by position. The data cube was produced using the PLAIT task and excluded unevenly-sampled edge regions. Observations covered the velocity range  $6552 \text{ km s}^{-1}$  to  $7425 \text{ km s}^{-1}$  with a velocity resolution of  $11 \text{ km s}^{-1}$ . The data cube was blanked using the AIPS<sup>7</sup> software package task BLANK resulting in a final cube containing 42 channels binned to a velocity resolution of  $21 \text{ km s}^{-1}$  with an angular resolution of 11.5 arcsec.

**Table 1.** HERA observational parameters

Rest frequency	$^{12}\text{CO}$ ( $J = 2 \rightarrow 1$ ) [GHz]	230.5
Sky frequency	[GHz]	225.3
Primary Beam	FWHP <sup>a</sup> [arcsec]	11.5
Primary Beam	FWHP [kpc]	4.5
Receivers	HERA	1 & 2
Backend channel width	[MHz]	2
$T_{\text{sys}}$	[K]	$300 \pm 100$
$\tau$ @ 225 GHz		$0.3 \pm 0.1$
Expected pointing accuracy	[arcsec]	2
$T_{\text{mb}}$		$1.73 T_A^*$

<sup>a</sup> Full width half power

## 3 OBSERVATIONAL RESULTS

The CO ( $J = 2 \rightarrow 1$ ) contours from the HERA integrated intensity map, in Figure 2 (top left), show that the bulk of CO ( $J = 2 \rightarrow 1$ ) was detected within a continuous emission region approximately  $16 \text{ arcsec}^2$  ( $7 \text{ kpc}^2$ ) in area, projected west and north of the optical centre. This continuous emission region is referred to as the “CO disk”. The CO disk contains the CO ( $J = 2 \rightarrow 1$ ) intensity maximum (CO maximum), indicated with yellow plus signs in Figure 2, and is located  $\sim 9.9 \text{ arcsec}$  (4.1 kpc) NW of the *Spitzer*  $4.5 \mu\text{m}$  intensity maximum ( $PA = 287^\circ$ ). Also marked in the same figure is a detached CO ( $J = 2 \rightarrow 1$ ) clump (CI)  $\sim 29 \text{ arcsec}$  (12 kpc) NW of the optical centre. CI is detected in 3 contiguous channels at  $> 3 \sigma$ . We are cautious about declaring CI a detection because of its low peak signal to noise (S/N)

<sup>7</sup> Astronomical Image Processing System

of 3.9, its lack of a counterpart at any other wavelength and its proximity to the map edge. However on balance its CO ( $J = 2 \rightarrow 1$ ) spectrum (Figure 3 – bottom left), CO ( $J = 2 \rightarrow 1$ ) single beam detection from Paper II, velocity and the total  $H_2$  mass including CI (see next paragraph) support CI being a real feature. The CO disk morphology of CGCG 97-079 differs dramatically from that of local spirals (Nishiyama et al. 2001; Leroy et al. 2009). If it followed that of the HERACLES nearby spiral sample (Leroy et al. 2009), it would display an exponential distribution with its origin at the optical centre with a typical expected scale length of  $0.23 r_{25}$  (i.e., 3.4 arcsec or 1.4 kpc).

$L(\text{CO})_{2-1}$  from the CO disk and CI is  $1.4 \pm 0.1 \times 10^8 \text{ K km s}^{-1} \text{ pc}^2$  ( $\Gamma_{\text{mb}}$  scale) which converted to an  $H_2$  mass, using equation B11<sup>8</sup> from Paper II ( $X$  factor of  $2.62 \times 10^{20} \text{ molecules cm}^{-2} / \text{K km s}^{-1}$ ), gives  $M(H_2) = 0.8 \pm 0.1 \times 10^9 M_{\odot}$ . This compares to the earlier  $H_2$  mass estimate based on single beam CO ( $J = 1 \rightarrow 0$ ) pointings (Paper II) of  $1.07 \times 10^9 M_{\odot}$ . Figure 2 – top left shows the position of the CO ( $J = 1 \rightarrow 0$ ) full width half power (FWHP) single beam pointings (dashed yellow circles), from which the earlier  $H_2$  mass was estimated. The HERA data presented here have a higher signal to noise. A comparison of spectra extracted from the current data with the single CO ( $J = 2 \rightarrow 1$ ) pointings from Paper II leads us to suspect the Paper II masses are less reliable. Further properties of the CO disk and CI are given in Table 2 with  $V_{\text{hel}}$ , and  $W_{20}$  calculated using the methods from Paper II.

Figure 3 (top left) shows the CO ( $J = 2 \rightarrow 1$ ) velocity field for the CO disk and CI in the regions where emission is  $> 3 \sigma$  in the integrated intensity map. From this velocity field and PV diagram (Figure 4 – top left) we see a systematic increase in velocity from  $6960 \text{ km s}^{-1}$  along an axis joining the optical centre and the CO ( $J = 2 \rightarrow 1$ ) intensity maximum where the velocity reaches  $7020 \text{ km s}^{-1}$ . From the CO ( $J = 2 \rightarrow 1$ ) maximum the velocity remains more or less constant between  $7020 \text{ km s}^{-1}$  to  $7040 \text{ km s}^{-1}$  out to the CI clump. A second velocity gradient is seen in the PV diagram, Figure 4 (top right), running NE ( $6936 \text{ km s}^{-1}$ ) to SW ( $7085 \text{ km s}^{-1}$ ) along an axis approximately aligned with knots D and knot E ( $PA \sim 244^\circ$ ). Knot identification letters follow the  $H\alpha$  knots from Gavazzi et al. (1995) as marked in Figure 2 (bottom left). This second PV diagram shows two velocity components, one at  $\sim 7000 \text{ km s}^{-1}$  and the other at  $\sim 7050 \text{ km s}^{-1}$ .

The HERA CO ( $J = 2 \rightarrow 1$ ) spectra for the CO disk, CI and a combined CO disk + CI spectrum are shown in Figure 3. The peak signal to noise (S/N) in the spectra are 6.8, 3.9, and 7.3, respectively. The CO ( $J = 2 \rightarrow 1$ ) velocity of the CO disk + CI ( $V = 7030 \pm 12 \text{ km s}^{-1}$ ) agrees within the errors with the H I velocity of  $7019 \pm 21 \text{ km s}^{-1}$  (Paper I) as does the HERA CO ( $J = 2 \rightarrow 1$ )  $W_{20}$  ( $240 \pm 25 \text{ km s}^{-1}$ ) and H I  $W_{20}$  ( $216 \pm 41 \text{ km s}^{-1}$ ), where  $W_{20}$  is the full width of the line at 20% of the peak emission in the spectrum.

<sup>8</sup> Equation B11 requires  $L(\text{CO})_{1-0}$  and to apply the equation we used the conversion:  $R21/R10 = 0.75$

## 4 DISCUSSION

In the following we summarise the properties of the gas and stellar components of CGCG 97-079, based on available data, including a series of papers by Gavazzi and collaborators (e.g., Gavazzi 1978; Gavazzi & Jaffe 1987; Boselli et al. 1994; Gavazzi et al. 1995, 2001; Boselli & Gavazzi 2014). We subsequently consider the scenarios most likely to explain the accumulated observations in the concluding remarks (section 5.)

### 4.1 The old stellar component

A combination of perturbed ISM and an unperturbed old stellar population is the key signature of an ongoing ram pressure stripping interaction (e.g., Kenney et al. 2004). Hubble Space Telescope imaging of ESO 137-001 which is suffering strong ram pressure stripping (Jáchym et al. 2014) shows narrow trails of blue optical emission, aligned downstream of the optical disk, as well as extra-planar dust above the inner part of the optical disk. So it is clear that extra-planar emission/absorption from dust mixed with the stripped gas as well as emission from young stars can result from ram pressure stripping. In general infrared (IR) emission is a better tracer of the old stellar population than optical emission. But IR emission from a galaxy’s old stellar population can be contaminated by dust re-emission following absorption of UV photons from recently formed high mass stars and stellar emission from RGB stars with ages of 10 to 100 Myr. Boselli et al. (2004) give the dust emission contamination at  $6.75 \mu\text{m}$  as up to 80% for Sc galaxies and 50% for blue compact dwarfs. But as Boselli et al. (2004) note MIR dust re-emission is more intense in massive quiescent galaxies than in star forming metal poor ones. CGCG 97-079 is both a dwarf and metal poor ( $Fe/H = -0.62$  Mouhcine et al. 2011). However, while contamination by dust re-emission is significant at mid infrared (MIR) wavelengths (including the  $6.75 \mu\text{m}$  and  $15 \mu\text{m}$ ) it is minimal in the *Spitzer*  $3.6 \mu\text{m}$  and  $4.5 \mu\text{m}$  (Fazio 2005; Utomo et al. 2014; Meidt et al. 2014). Modelling by Utomo et al. (2014) indicates the contamination (including from polycyclic aromatic hydrocarbon) remains minimal (of the order of a few %) at  $3.6 \mu\text{m}$  and  $4.5 \mu\text{m}$  even for galaxies with  $H\alpha$  equivalent widths ( $EW$ ) similar to CGCG 97-079 ( $EW(H\alpha) = 129$  per GOLDMine). For a disk galaxy contamination from young stellar emission (principally from red supergiants) at  $\sim 2.3 \mu\text{m}$  is estimated at  $\sim 3\%$ , but in star forming regions within the galaxy the contamination can be as high as 33% (Rhoads 1998). The strength of the emission from red supergiants in the wavelength range of  $2.3 \mu\text{m}$  and  $4.5 \mu\text{m}$  declines with increasing wavelength (Baron et al. 2014). This suggests that red supergiant contamination at  $4.5 \mu\text{m}$  is likely to be less than at  $2.3 \mu\text{m}$  by a factor of a few. Because of the non-availability of a *Spitzer*  $3.6 \mu\text{m}$  image we were unable to make the polycyclic aromatic hydrocarbon (PAH) and young stellar emission contamination corrections developed by (Meidt et al. 2012, 2014). We conclude that in the absence of these corrections the  $4.5 \mu\text{m}$  band image provides the best available, tracer of the old stellar population. This band is known to suffer some CO absorption (Meidt et al. 2014).

Figure 2 (bottom right) shows the *Spitzer*  $4.5 \mu\text{m}$  image for CGCG 97-079, with contours from the same image with

**Table 2.** CO ( $J = 2 \rightarrow 1$ ) properties from HERA

Property	Unit	CO disk	CI	Disk + CI
$L(\text{CO})_{2-1}$ [ $T_{\text{mb}}$ ]	[ $\text{K km s}^{-1} \text{pc}^2$ ]	$1.2 \pm 0.1 \times 10^8$	$0.2 \pm 0.05 \times 10^8$	$1.4 \pm 0.1 \times 10^8$
$M(\text{H}_2)$	[ $10^9 M_{\odot}$ ]	$0.7 \pm 0.1$	$0.1 \pm 0.03$	$0.8 \pm 0.1$
$V_{\text{hel}}$	[ $\text{km s}^{-1}$ ]	$7000 \pm 13$	$7045 \pm 31$	$7030 \pm 12$
$W_{20}$	[ $\text{km s}^{-1}$ ]	$220 \pm 26$	$210 \pm 62$	$240 \pm 25$
rms per channel [ $T_{\text{mb}}$ ]	[mK]			3.1
rms integrated map [ $T_{\text{mb}}$ ]	[ $\text{K km s}^{-1}$ ]			0.23

a 3-pixel wide boxcar smoothing applied. The un-smoothed image had a pixel size = 1.2 arcsec and resolution  $\sim 2.5$  arcsec). Two principal intensity maxima are seen in the figure: an infrared counterpart to  $\text{H}\alpha$  knot A, and a more elongated counterpart approximately coinciding with  $\text{H}\alpha$  knots B and C. The  $4.5 \mu\text{m}$  intensity maximum is projected at approximately the same position as the optical centre and knot B. The figure shows the intensity of the  $4.5 \mu\text{m}$  emission falls steadily south of the optical centre, but to the N and NW of it there is an extensive region of diffuse emission. An uncatalogued  $4.5 \mu\text{m}$  feature marked F on the figure is not present in the 2MASS, optical (SDSS) or  $\text{H}\alpha$  images, although it does have a counterpart in our  $J$  - band image obtained with the SPM<sup>9</sup> 2.1 m telescope. Knot F's colour suggests it is a higher redshift background galaxy. The optical counterparts of the two objects in the same figure  $\sim 10$  arcsec N of knot F are catalogued as 23rd magnitude stars in SDSS.

Depending on the weighting given to the high and low intensity  $4.5 \mu\text{m}$  emission there are several possible alternative inclinations and morphologies for the old stellar disk. Three possible old stellar disk orientations are over plotted as ellipses in Figure 5. The yellow ellipse represents an edge-on,  $\sim 90^\circ$  inclination disk ( $PA = 275^\circ$ ) aligned with knots A, B, C and D, the dashed white ellipse is a lower inclination ( $60^\circ$ ) disk ( $PA = 286^\circ$ ) aligned with the outer edges of the detected  $4.5 \mu\text{m}$ , and the solid white ellipse represents an edge on,  $\sim 90^\circ$  inclination disk ( $PA = 286^\circ$ ) aligned with knots B and C. In case of the high inclination disk options the diffuse  $4.5 \mu\text{m}$  emission to the north of the optical centre, and particularly the upward curve at the western disk edge, would be evidence of a tidal perturbation. On the other hand for the lower inclination ( $60^\circ$ ) disk the northern diffuse emission would just be part of the disk. Because of these and further alternative interpretations of the  $4.5 \mu\text{m}$  data, as well as our inability to make the PAH and young stellar emission contamination corrections, we were unable to definitively determine whether the morphology of the old stellar disk is perturbed or not.

## 4.2 HI and CO gas components

CGCG 97-079 is particularly gas rich, with  $M(\text{H}_2 + \text{H I} + \text{He}) = 2.9 \times 10^9 M_{\odot}$  ( $M_{\text{HI}} = 1.3 \times 10^9 M_{\odot}$  - Paper I) and taking  $M_* = 1.2 \times 10^9 M_{\odot}$  gives a gas fraction<sup>10</sup>,  $f_{\text{gas}} = 0.7$ . Its  $M(\text{H I})/M_* = 1.25$  is consistent with that found for dwarf (Zhang et al. 2012) and smaller late-type galaxies (Cortese et al. 2011) like the LMC and M33. Based on the

HERA observations the  $\text{H}_2$  excess (including CI) is -0.50, in good agreement with the  $\text{H}_2$  excess from Paper II (-0.64). As discussed in Paper II, there are significant uncertainties both in the determination of the  $\text{H}_2$  mass of individual galaxies and the calibration of  $\text{H}_2$  deficiencies from samples of unresolved CO observations, but based on the available data we can, at a minimum, conclude that CGCG 97-079 is not deficient in molecular gas. Gavazzi et al. (2001) estimated the mass of  $\text{H}\alpha$  in the ionised tail as  $9.6 \times 10^8 M_{\odot}$ , which could account for almost all of the H I deficiency (0.25) reported for CGCG 97-079 in Paper I, provided the  $\text{H}\alpha$  emission is from gas that was originally H I stripped from the galaxy. The NW offset of the CO ( $J = 2 \rightarrow 1$ ) distribution from the optical centre, presented in section 3, is further illustrated in Figure 4 (lower panel), which shows the normalised CO ( $J = 2 \rightarrow 1$ ) emission integrated along the axis of knots B and C in comparison with  $4.5 \mu\text{m}$  emission along the same axis. The displacement of the CO ( $J = 2 \rightarrow 1$ ) from the highest density old stellar component of the galaxy is clearly seen in the figure.

Figure 2 (top right) shows that the H I intensity maximum from the VLA C-array is offset by 7 arcsec (3 kpc) north-west of the CO ( $J = 2 \rightarrow 1$ ) maximum and has a column density derived from the VLA data (C+D-array) of  $6.6 \times 10^{20} \text{ atom cm}^{-2}$  (Hota & Saikia 2007). This offset is consistent with our deeper VLA - D array observation in Paper I. The Hota VLA data (C+D-array) map (their figure 14) shows the H I velocities increasing from  $6923 \text{ km s}^{-1}$  in the NE to  $7117 \text{ km s}^{-1}$  in the SW along the knot E to D axis. A similar CO ( $J = 2 \rightarrow 1$ ) velocity gradient is observed along the same axis and the CO ( $J = 2 \rightarrow 1$ ) PV diagram for a cut along this axis indicates there are two velocity components (Section 3). Also detailed in section 3 is the CO ( $J = 2 \rightarrow 1$ ) velocity gradient between the optical centre and the CO ( $J = 2 \rightarrow 1$ ) maximum with a decrease in the gradient NW of the CO ( $J = 2 \rightarrow 1$ ) maximum.

Both the offsets of the H I and CO ( $J = 2 \rightarrow 1$ ) maxima from the optical/ $4.5 \mu\text{m}$  centre and the segregation of the high column density H I and CO ( $J = 2 \rightarrow 1$ ) maxima contrast with NGC 4522 and NGC 4330 in the Virgo cluster (Vollmer et al. 2008, 2012), where the high column density H I and CO remain projected at the optical centre during ram pressure stripping. Although NGC 4522 and NGC 4330 are both significantly more massive than CGCG 97-079.

## 4.3 Recent star formation

$\text{H}\alpha$  (Figure 2, bottom left) and FUV *GALEX* (Figure 6) emission trace star formation on time scales of  $10^7$  yr and  $10^8$  yr respectively (Boselli et al. 2009) and are both concentrated east of the CO ( $J = 2 \rightarrow 1$ ) maximum. About 30% of the CGCG 97-079 FUV emission is detected within

<sup>9</sup> San Pedro Mártir, Mexico (Observatorio Astronómico Nacional)

<sup>10</sup> Ratio of gas mass to the sum of gas and stellar masses.

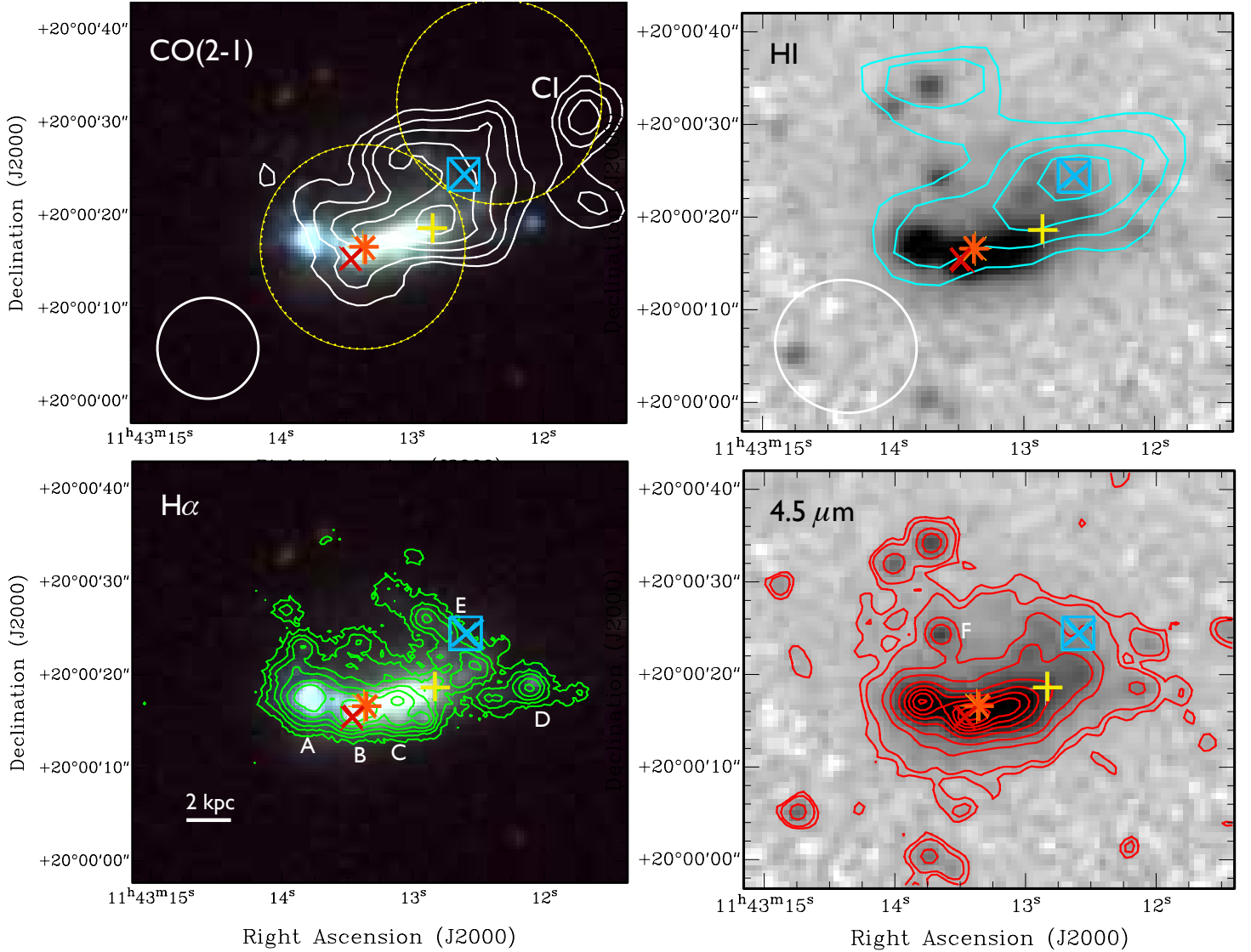


**Figure 2.** CGCG 97-079 *top left*: CO ( $J = 2 \rightarrow 1$ ) HERA integrated intensity map contours (gray) overlaid on a composite SDSS false colour  $g, r, i$  band image. The first contour level is at  $3 \sigma$ , equivalent to  $0.68 \text{ K km s}^{-1}$  ( $T_{\text{mb}}$ ) and subsequent contours are at 1.0, 1.3, 1.7, and  $2.0 \text{ K km s}^{-1}$  ( $T_{\text{mb}}$ ). The white circle indicates the size of the CO ( $J = 2 \rightarrow 1$ ) beam and CI indicates the position of the detached clump. The IRAM 30-m 22 arcsec FWHP single beams for the CO ( $J = 1 \rightarrow 0$ ) Paper I observations at the optical centre and offset  $RA = -15.6$  arcsec,  $DEC = 15.6$  arcsec are indicated with large dashed yellow circles. *Top right*: H I (VLA C-array) contours (cyan) overlaid on a  $4.5 \mu\text{m}$  image (resolution  $\sim 2$  arcsec). The contours are at 2, 2.5, 3, and  $3.5 \sigma$ . The white circle indicates the size of the VLA C-array beam. *Bottom left*:  $H\alpha$  contours (green) from GOLDMine (resolution  $\sim 3$  arcsec) overlaid on a composite SDSS false colour  $g, r, i$  band image. The contours are at 20, 50, 100, 200, 400 and  $800 \sigma$ . The letters A to E mark the 5 principal H II regions ( $H\alpha$  knots), following the naming convention from Figure 2 of (Gavazzi et al. 1995). *Bottom right*: *Spitzer* contours from a  $4.5 \mu\text{m}$  boxcar smoothed image, overlaid on a  $4.5 \mu\text{m}$  un-smoothed image. The contours are at 4.5, 5.5, 10, 15, 25, 35, 45, 55, 65 and  $75 \sigma$  with the  $4.5 \sigma$  contour equivalent to  $0.085 \text{ MJy sr}^{-1}$ . The resolution of the  $4.5 \mu\text{m}$  image is  $\sim 2.5$  arcsec. The orange asterisk marks the optical centre and the cyan 'X' in box marking the position of the H I intensity maximum from the VLA C-array. The red 'X' corresponds to the  $4.5 \mu\text{m}$  maximum and the yellow plus symbol the CO ( $J = 2 \rightarrow 1$ ) maximum from the HERA map.

a radius of  $\sim 3$  arcsec (1.25 kpc) of knot A. The  $H\alpha$  emission is concentrated in knots A, B and C. These three knots are also the source of the strongest 1.5 GHz radio continuum emission (Figure 1b in Gavazzi et al. 1995). Figure 7 shows a  $g - i$  band image produced from SDSS  $g$  and  $i$

band background subtracted images overlaid with HERA CO ( $J = 2 \rightarrow 1$ ) contours. From the figure we see an extensive area between knots B and E with  $g - i \sim 0.7$ . The figure shows this area correlates well with the high column density CO ( $J = 2 \rightarrow 1$ ) emission. This strongly suggests

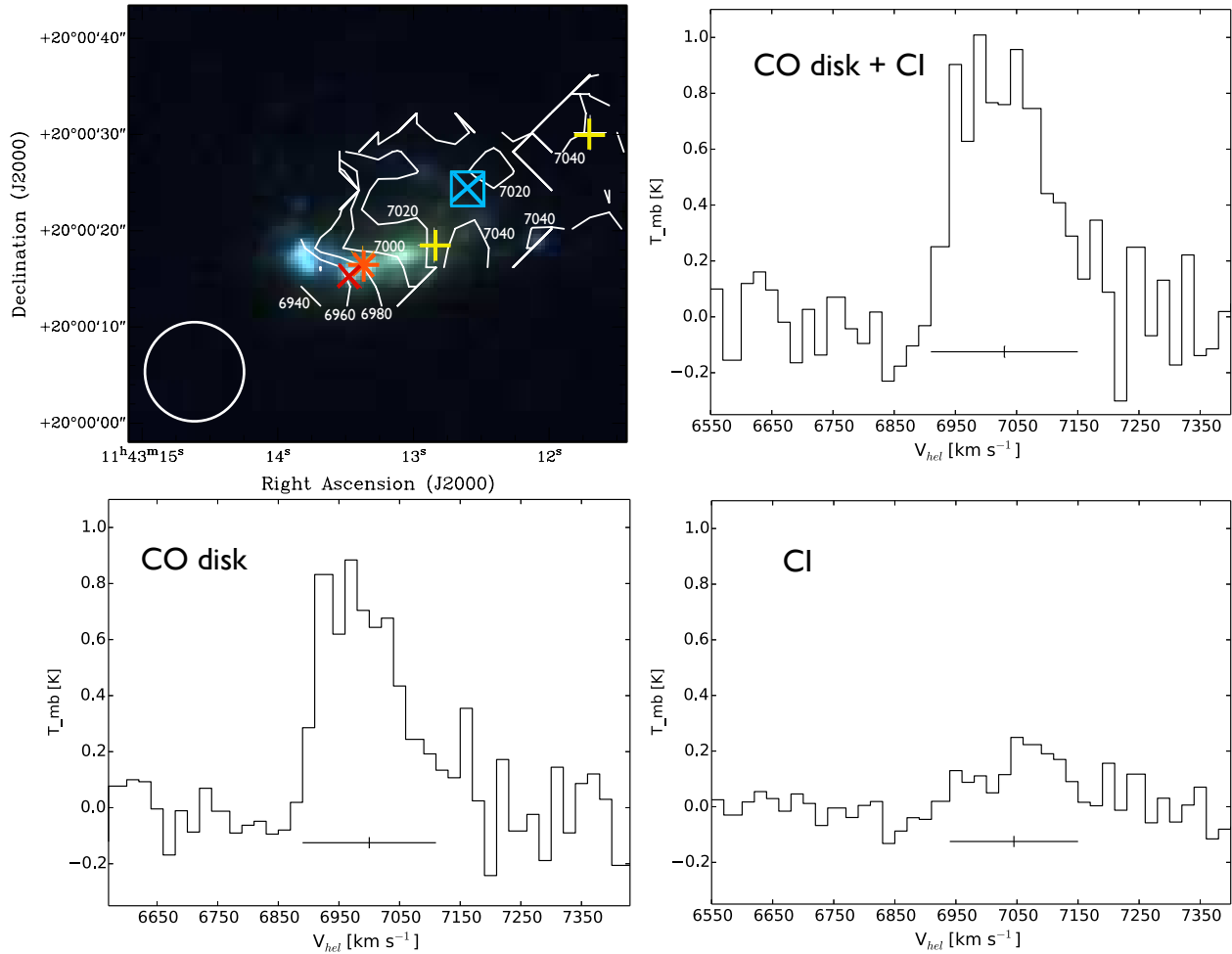


**Figure 3.** *Top left panel:* CO ( $J = 2 \rightarrow 1$ ) velocity map with contours ( $\text{km s}^{-1}$ ) overlaid on a composite SDSS  $g, r, i$  band image. The white circle at the bottom left of the panel shows the approximate size of the HERA CO ( $J = 2 \rightarrow 1$ ) beam. The colours and symbols are as in Figure 2 except the yellow plus symbol at the top right which marks CI. *Top right panel:* HERA CO ( $J = 2 \rightarrow 1$ ) spectra for the CO disk + CI. *Bottom left panel:* HERA CO ( $J = 2 \rightarrow 1$ ) spectrum for the CO disk. *Bottom right panel:* HERA CO ( $J = 2 \rightarrow 1$ ) spectrum for CI. The  $T_{\text{mb}}$  for each channel in a spectrum ( $21 \text{ km s}^{-1}$  velocity width per channel) is the sum of the  $T_A^*$  for all pixels in the channel, converted to the  $T_{\text{mb}}$  scale. The horizontal line at the bottom of each spectrum indicates the spectrum’s  $W_{20}$  velocity width and the vertical cross bar the  $V_{\text{hel}}$ .

the  $g - i$  value in this region is the result of dust extinction and the bluer  $g - i$  colours for knots A and D are partially the result of lower extinction compared to knots B and C. Even allowing for this, knot D appears to be dominated by a younger population of stars than the four other knots. An interesting feature in the  $\text{H}\alpha$  image is the ridge of  $\text{H}\alpha$  emission along the knot E to D axis ( $PA = 244^\circ$ ) which has less well defined optical (SDSS),  $4.5 \mu\text{m}$ ,  $\text{H I}$  and CO ( $J = 2 \rightarrow 1$ ) counterparts.

#### 4.4 High impact low velocity tidal interactions with nearby neighbours

Here we consider whether there is a neighbouring galaxy or galaxies which could have tidally disrupted CGCG 97-079 within the last few  $\times 10^8$  yr assuming a typical group ve-

locity of  $\sim 250 \text{ km s}^{-1}$ . To try to identify any such galaxy we used a modified version of the tidal force ( $Q$ ) and number density ( $\eta = 2.5$ ) parameters from Verley et al. (2007), applied to data from SDSS DR8. A  $Q < 0$  indicates the gravitational forces within the galaxy exceed the gravitational force exerted by the neighbours. We find  $Q = -1.10$  for the 27 neighbours in the western sub-cloud of the NW sub-cluster (Cortese et al. 2004) and  $Q = -1.25$  for the nearest neighbour, A 1367 GP82 1236 (see Figure 1 at  $RA = 11^{\text{h}}43^{\text{m}}10.961^{\text{s}}$ , and  $DEC = +20^\circ01'47.01''$ ). The tidal perturbation parameter<sup>11</sup>  $p_{gg} = 0.004$  for CGCG 97-079 with

<sup>11</sup>  $p_{gg} = \frac{(M_{\text{comp}}/M_{\text{gal}})}{(d/r_{\text{gal}})^3}$  where  $M_{\text{gal}}$  and  $M_{\text{comp}}$  are the masses of the galaxy and companion respectively,  $d$  is the separation and  $r$  is the galaxy disk radius (Byrd & Valtonen 1990), where values of  $p_{gg} > 0.1$  likely lead to tidally induced star formation.

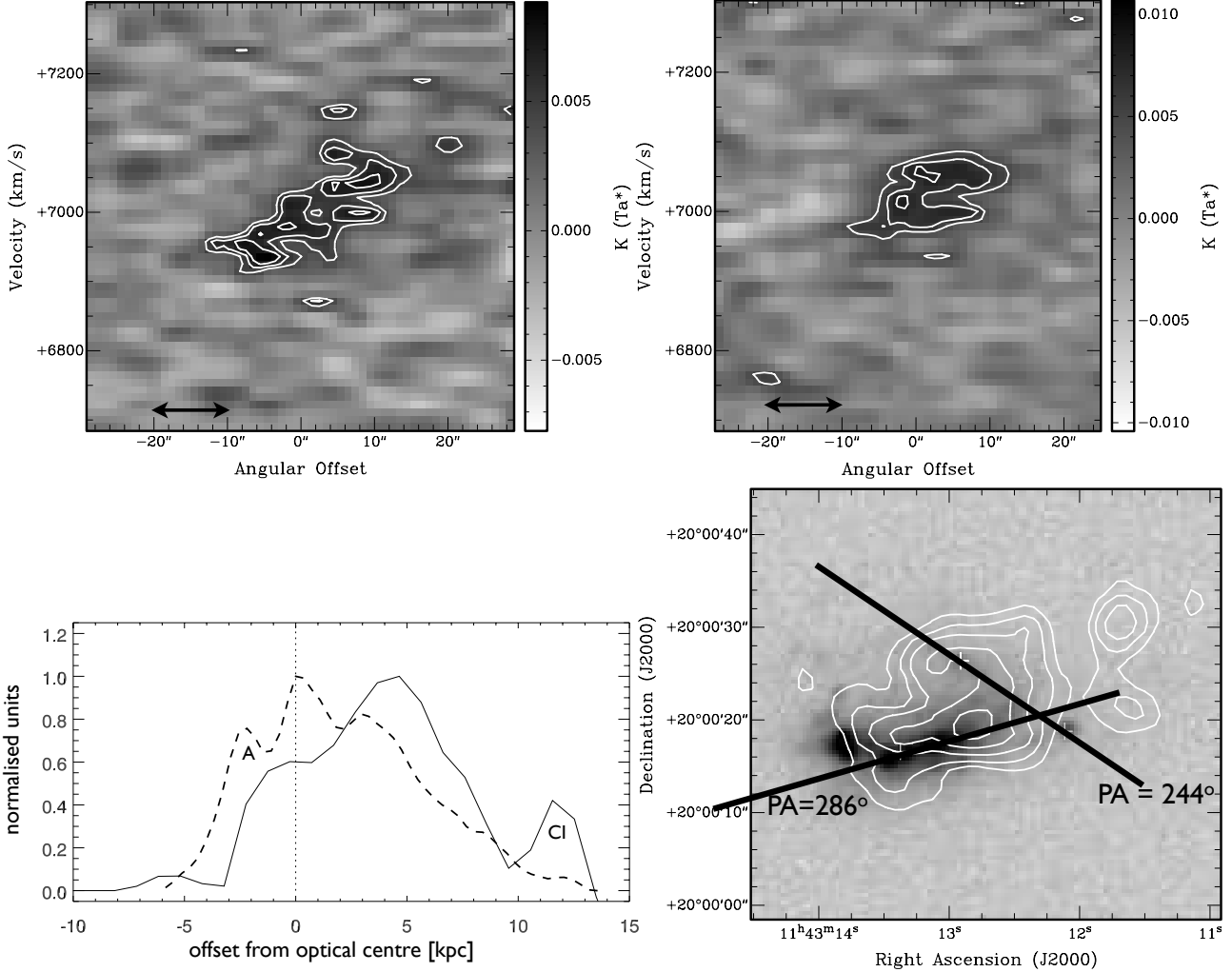


**Figure 4.** *Top left panel:* PV diagram ( $PA = 286^\circ$ ) centred at the optical centre. The angular offset, in arcsec, is negative to the SE (left) and positive to the NW (right). *Top right panel:* PV diagram ( $PA = 244^\circ$ ) along the line connecting knot E and D centred at knot E. The angular offset, in arcsec, is negative to the NE (left) and positive to the SW (right). The horizontal arrows indicated the size of the HERA beam. *Bottom left panel:* CGCG 97-079 integrated *Spitzer* IRAC 4.5  $\mu\text{m}$  (dashed line) and CO ( $J = 2 \rightarrow 1$ ) (solid line) emission in normalised units along the  $PA = 286^\circ$  centred on the optical centre of the galaxy. The horizontal axis shows the offset from the optical centre in kpc, with positive values to the NW. *Bottom right panel:* SDSS g – band image showing the orientation and lengths of the slices along which the PV diagrams were derived.

A 1367 GP82 1236 is more than an order of magnitude below that expected to produce detectable molecular gas perturbations in CGCG 97-079. We conclude from both the  $Q$  and  $p_{gg}$  parameters and evidence that the perturbation occurred within  $\sim 10^8$  yr (section 4.5), that the substantial displacement of the high column density molecular gas in CGCG 97-079 is unlikely to be due to a low velocity high impact tidal interaction with A 1367 GP82 1236.

#### 4.5 High velocity interactions

In this section we consider whether CGCG 97-079 may have undergone a recent high velocity ( $\sim 1000 \text{ km s}^{-1}$ ) hydrodynamic and/or tidal interaction. If the perturbation that

caused H I and CO maxima offsets also drove the recent evolution of the stellar population we can infer the elapsed time since the interaction from the galaxy’s integrated properties. GALEV evolutionary synthesis models (Kotulla et al. 2009) with realistic parameters produce a set of solutions for the observed  $M_* = 1.2 \times 10^9 M_\odot$  and  $SFR = 1.06 M_\odot \text{ yr}^{-1}$  (Paper II) for star bursts with burst strengths of  $\sim 0.20 - 0.25$ . The model constraint on these solutions from the optical and NIR colours is rather poor, using either the GALEV or FUV based Milky Way + internal extinction, but favour solutions with a time since the star burst of several  $\times 10^7$  yr to a few  $\times 10^8$  yr. The expected relaxation time scales for perturbed CO ( $J = 2 \rightarrow 1$ ) and H I (Holwerda et al. 2011)



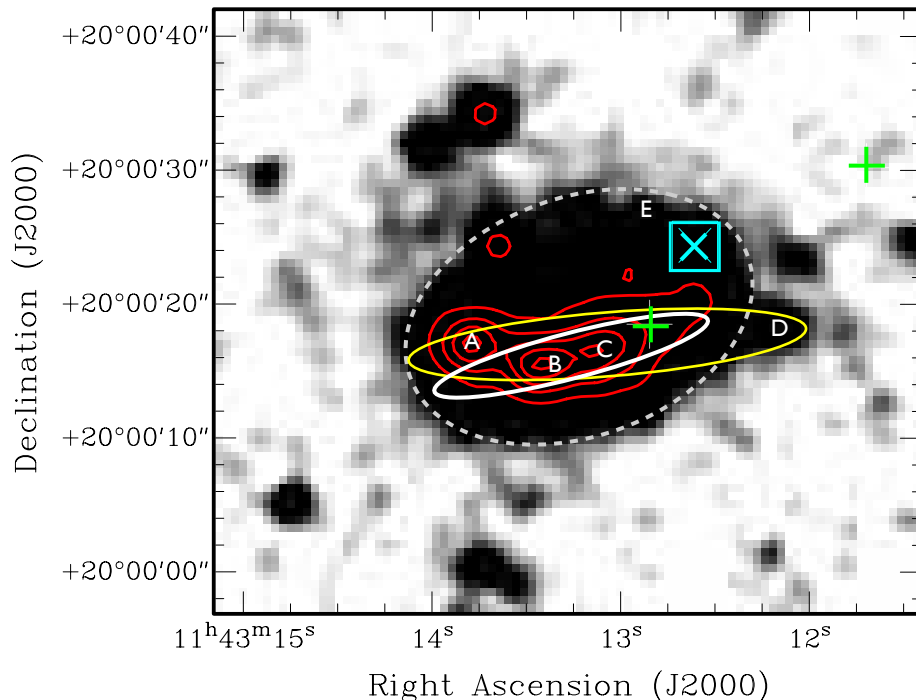


**Figure 5.** Stretched  $4.5 \mu\text{m}$  band image of CGCG 97-079. The ellipses indicate three possible pre-interaction stellar disks: the yellow ellipse represents a edge on,  $\sim 90^\circ$  inclination, disk ( $PA = 275^\circ$ ) encompassing knots A, B, C and D; the white dashed ellipse is a lower inclination ( $\sim 53^\circ$ ) inclination disk ( $PA = 290^\circ$ ) tracing the outer edges of  $4.5 \mu\text{m}$  - band emission; and the solid white ellipse represents an edge on,  $\sim 90^\circ$  inclination, disk ( $PA = 286^\circ$ ) aligned with knots B and C. The cyan X in box marks the position of the H I intensity maximum from the VLA C-array and the green plus symbols the CO ( $J = 2 \rightarrow 1$ ) maximum and CI from the HERA map. The knot names are the same as used in Figure 2.

together with GALEV modelling indicate the perturbation of the galaxy probably occurred  $\sim 10^8$  yr ago.

The deep H $\alpha$  image of CGCG 97-079 and CGCG 97-073 in (Boselli & Gavazzi 2014, their figure 21) shows each galaxy to have a spectacular H $\alpha$  tail extending  $\sim 100$  kpc and 70 kpc from their respective optical disks and meeting in projection at  $\sim 11:42:57.7, +20:02:29.42$  (see Figure 1). At the vertex of the H $\alpha$  tails the complex H $\alpha$  morphology strongly suggests a high velocity tidal encounter occurred between the two galaxies earlier in their infall to the cluster as proposed in Gavazzi et al. (2001). There are indications in Boselli et al. (1994) (at low significance) and Sivanandam et al. (2014) that the molecular gas in CGCG 97-073 is also offset in the direction of its tail. Assuming the most recent star burst in CGCG 97-079 was driven by the interaction at the tail intersection between  $\sim 7 \times 10^7$  yr to  $2 \times 10^8$  yr ago (as indicated by the GALEV models), the CGCG 97-079 projected H $\alpha$  tail length ( $\sim 4.3$  arcmin – 106 kpc), implies a velocity in the plane of the sky in the range of  $500 \text{ km s}^{-1}$  to  $1500 \text{ km s}^{-1}$  in agreement with the  $1200 \text{ km s}^{-1}$  velocity and  $10^{7.8}$  yr derived by Gavazzi et al. (2001) for the survival time of the ionised tail.

Simple modelling of ram pressure at CGCG 97-079's distance from the NW sub-cluster core (Paper I) implies  $P_{\text{ram}} \approx 10^{-11} \text{ dyn cm}^{-2}$  for a  $V_{\text{rel}}$  of  $1000 \text{ km s}^{-1}$ . CGCG 97-079 remains gas rich ( $f_{\text{gas}} = 0.7$ ) with no overall gas deficiency (although marginally H I deficient) despite evidence

from the H $\alpha$  tails that ram pressure stripping has operated for least  $\sim 1 \times 10^8$  yr. This, the indication from section 4.2 that most of the stripped H I is now observed in the H $\alpha$  tails and the estimate of  $P_{\text{ram}} \approx 10^{-11} \text{ dyn cm}^{-2}$  all indicate CGCG 97-079 has suffered only moderate ram pressure stripping. Further support for moderate ram pressure comes from the absence of an H I counterpart to the H $\alpha$  tail. Based on our VLA – D observations from Paper I we estimate there could at most be  $3 \times 10^8 M_\odot$  of H I undetected in the tail, i.e. the H $\alpha$  + potential undetected H I in the tail account for the H I deficiency.

Ram pressure stripping models have usually been applied to more massive and earlier Hubble-type spirals with classical bulges and lower gas fractions (e.g., spirals with  $M_* = 3.8 \times 10^{10} M_\odot$  and  $f_{\text{gas}} = 0.08$ ; Roediger & Hensler 2005). At  $P_{\text{ram}} = 10^{-11} \text{ dyn cm}^{-2}$  the presence/absence of a bulge does not impact the stripping efficiency (Steinhauser et al. 2012). But modelling of the ram pressure stripping of gas rich dwarves ( $M_* = 0.6 \times 10^9 M_\odot$ ) by Marcolini et al. (2003) have complete gas stripping time scales of between  $2 - 4 \times 10^8$  yr for ram pressures at least an order of magnitude below that predicted for CGCG 97-079 at  $V_{\text{rel}} = 1000 \text{ km s}^{-1}$ .

Confirmation of the ability of ram pressure stripping to remove almost all of the gas from a dwarf on timescales of a few  $\times 10^8$  yr comes from the study of IC 3418 (Kenney et al. 2014). IC 3418 is a highly H I deficient Irr dwarf in Virgo pro-

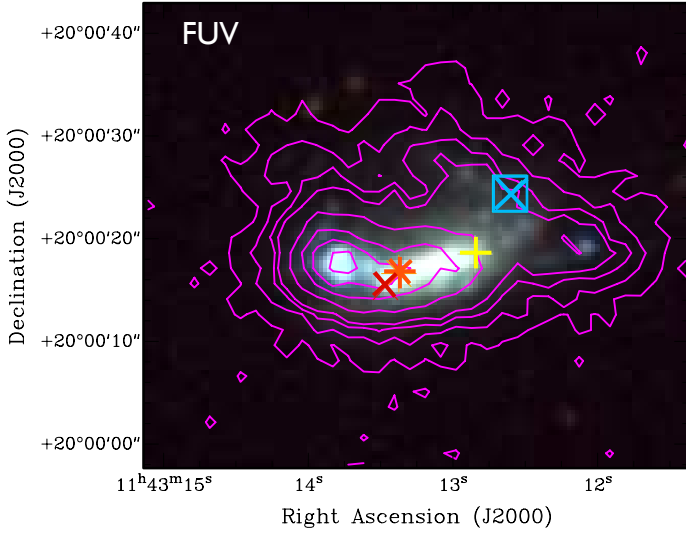


**Figure 6.** CGCG 97-0979: Contours from a FUV (*GALEX*) image, overlaid on a composite SDSS false colour *g, r, i* – band image. The contours are at 4, 15, 30, 45, 60, 100, 200, 300 and 400  $\sigma$  with the 4  $\sigma$  equivalent to  $1.74 \times 10^{-18}$  erg sec $^{-1}$  cm $^{-2}$  Å $^{-1}$ . The resolution of the FUV image is  $\sim 4$  arcsec.

jected 225 kpc from M87, with  $\sim 1/3$ rd of the stellar mass of CGCG 97-079. The galaxy is thought to have undergone rapid ram pressure stripping within the last few  $\times 10^8$  yr which truncated its star formation. CO was marginally detected in the disk, which together with evidence of super giant star formation  $\leq 10^8$  yr ago in the stellar disk, supports the proposition that the highest density gas remains within a dwarf’s disk until ram pressure stripping is complete. H I in IC 3418 was only detected within the starforming tail.

Given CGCG 97-079 has a stellar mass, a gas fraction and other properties which are similar to dwarves as well as the evidence ram pressure stripping has operated for at least  $10^8$  yr, we conclude that had CGCG 97-079 been subject to continuous ram pressure much stronger than predicted from Paper I (say  $P_{\text{ram}} = \sim 1 \times 10^{-10}$  dyn cm $^{-2}$ ) or its lower mass compared to generalised ram pressure models produced significantly more efficient H I stripping, a substantial overall gas deficiency and H I tail would be observable by now. Since neither this deficiency nor an H I tail is observed, steady ram pressure seems unlikely to be the principal cause of the offsets between the H I, CO ( $J = 2 \rightarrow 1$ ) and stellar intensity maxima. However a sudden increase in ram pressure from a rapid increase in ICM density, such as that proposed for NGC 4522 (Kenney et al. 2004), might have led to the displacement of the H I and CO ( $J = 2 \rightarrow 1$ ) with respect to the stellar maxima without sufficient time for gas deficiencies or an H I tail to develop. Such an increase in ram pressure might arise from shocks or ICM substructure which are more likely in a merging cluster, although the X-ray (*XMM*) data does not show evidence of an ICM density enhancement at or close to CGCG 97-079. For the ram pressure stripping archetype NGC 4522 there is no indication that the highest

density CO ( $J = 2 \rightarrow 1$ ) was displaced from its currently observed location (in a disk surrounding the optical centre) during the proposed spike in ram pressure. Although there is kinematic evidence that some H I has fallen back subsequently (Kenney et al. 2004). The argument that a similar order of magnitude spike in ram pressure is the cause of the observed separation of the highest density CO ( $J = 2 \rightarrow 1$ ), H I and stellar components in CGCG 97-079 would therefore rely on this being the consequence of the shallower potential in CGCG 97-079 compared to NGC 4522.

## 5 CONCLUDING REMARKS

CGCG 97-079 is a large gas rich dwarf with a modest H I deficiency and a significant H $_2$  excess which displays complex morphology (and gas kinematics) at each of the wavelengths considered above. Taken together these clearly indicate the galaxy has suffered a strong perturbation. This perturbation probably coincided with a burst of star formation which evolutionary synthesis models indicate occurred  $\sim 10^8$  yr ago.

CGCG 97-073 and CGCG 97-079 display impressive  $\sim 70$  and 100 kpc H $\alpha$  tails respectively in the deep Boselli & Gavazzi (2014) H $\alpha$  image which meet each other in projection NW of CGCG 97-079. Modelling in Gavazzi et al. (2001) suggests a high-speed tidal interaction, at the vertex of the H $\alpha$  tails, subsequently enhanced the efficiency of ram pressure stripping of H I from both galaxies. The H $\alpha$  tails of both galaxies only become visible in the deep Boselli & Gavazzi (2014) H $\alpha$  image from the tails’ vertex onwards. Prior to the high-speed tidal interaction, ram pressure stripping was insufficient to produce detectable H $\alpha$  tails, i.e., both tails are detectable because the high-speed interaction “loosened” gas in the disks, which following stripping and ionisation now present as the H $\alpha$  tails. The time scale for the high-speed interaction assuming a  $V_{\text{rel}}$  of 1000 km s $^{-1}$  (which implies a current  $P_{\text{ram}} = 10^{-11}$  dyn cm $^{-2}$ ) is  $10^8$  yr in good agreement with the time since the last burst of star formation and the timescale from the Gavazzi et al. (2001) modeling. Based on the analysis in section 4.4 we concluded that H I, CO ( $J = 2 \rightarrow 1$ ) and stellar intensity maxima offsets (maxima offsets) are not the result of a high impact low velocity interaction with a near neighbour. We also investigated whether the maxima offsets could be the result of a recent minor merger but did not find convincing evidence for this. A further possibility is the ram pressure stripping of gas has caused a shift in the cusp of the dark matter halo away from the centre of the dark matter (DM) halo via drag forces. This effect was modelled for a medium mass (total mass =  $10^{10}$  M $_{\odot}$ ) dwarf subject to face-on ram pressure stripping by (Smith et al. 2012). Their model with a similar  $f_{\text{gas}}$  (0.5) and ram pressure to that calculated for CGCG 97-079 predicts a shift in the cusp and stellar disk centres from the centre of the DM halo of  $< 0.5$  kpc on time scales of  $10^8$  yr. But more critically in their models the gas within the truncation radius remains bound to the deepest potential of the DM, i.e., this mechanism is unlikely to explain the high density offsets. The most likely remaining possibilities are that the offsets in neutral and molecular ISM are the result of ram pressure and/or were produced by the high-speed interaction with CGCG 97-073. As we note in the introduction models and observations of spirals more mas-

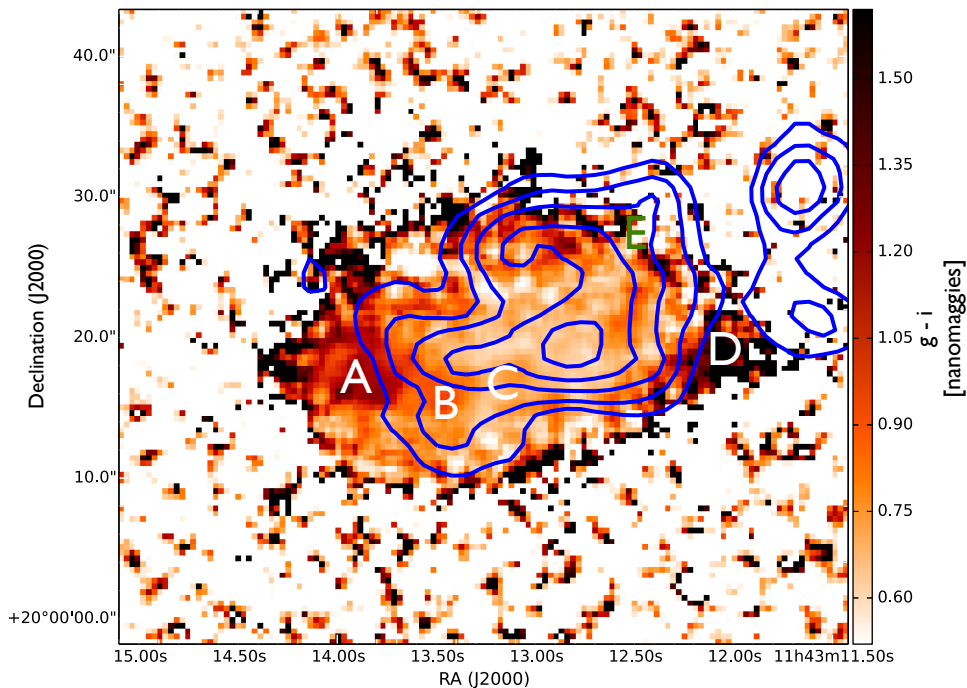


**Figure 7.** CGCG 97-079 SSDS  $g - i$  band image with the same CO ( $J = 2 \rightarrow 1$ ) contours (blue) and H $\alpha$  knot identifications as in Figure 2.

sive than CGCG 97-079 indicate the estimated ram pressure of  $P_{\text{ram}} = 10^{-11} \text{ dyn cm}^{-2}$  alone would not produce such offsets. Unlike ram pressure stripping, tidal interactions are known to be capable of affecting high density H I and molecular gas located deep within the galactic gravitational potential well (Duc & Mirabel 1994; Iono et al. 2005) and the relaxation time scale for H I is  $> 1 \times 10^8 \text{ yr}$  (Holwerda et al. 2011). High velocity "harassment" type fly-by interactions in higher mass spirals than CGCG 97-079 are expected to have only a minimal impact on the old stellar component (Duc & Bournaud 2008), but it is unclear whether this also the case for lower mass spirals such as CGCG 97-079. For the CGCG 97-079 / CGCG 97-073 we do not know whether the interaction between them was a fly-by or the disks penetrated each other.

In summary without clear evidence of the impact of the interaction on the old stellar disk (section 4.1) and the uncertainty about whether the shallower gravitational potential in CGCG 97-079, compared to the best studied cases, could allow ram pressure or a high-speed tidal interaction to produce the observed maxima offsets, we are unable to determine whether ram pressure or a high-speed tidal interaction was the principal cause of the observed maxima offsets. However ram pressure stripping is likely to be playing a significant role in the perturbation of lower density gas. Resolved ram pressure stripping modeling of the ISM in spirals with masses similar to CGCG 97-079 would greatly assist in resolving this question.

## ACKNOWLEDGMENTS

We are grateful to the anonymous referee for his/her helpful and insightful comments which have, significantly improved the paper. We would also like to thank Nicola Brassington, Elke Roediger and Martin Hardcastle for very useful discussions. LC acknowledges support under the Australian Research Council's Discovery Projects funding scheme (DP130100664). HBA acknowledges support for this project via CONACyT grant No. 50794. This research has made use of the NASA/IPAC Extragalactic Database (NED) which is operated by the Jet Propulsion Laboratory, California Institute of Technology, under contract with the National Aeronautics and Space Administration.

This research has made use of the Sloan Digital Sky Survey (SDSS). Funding for the SDSS and SDSS-II has been provided by the Alfred P. Sloan Foundation, the Participating Institutions, the National Science Foundation, the U.S. Department of Energy, the National Aeronautics and Space Administration, the Japanese Monbukagakusho, the Max Planck Society, and the Higher Education Funding Council for England. The SDSS Web Site is <http://www.sdss.org/>.

## REFERENCES

- Baron F., Monnier J. D., Kiss L. L., Neilson H. R., Zhao M., Anderson M., 2014, *ApJ*, 785, 46
- Boselli A., Boissier S., Cortese L., Buat V., Hughes T. M., Gavazzi G., 2009, *ApJ*, 706, 1527

- Boselli A., Cortese L., Boquien M., Boissier S., Catinella B., Gavazzi G., Lagos C., Saintonge A., 2014, *A&A*, 564, A67
- Boselli A., Gavazzi G., 2006, *PASP*, 118, 517
- Boselli A., Gavazzi G., 2014, 22, 74
- Boselli A., Gavazzi G., Combes F., Lequeux J., 1994, *A&A*, 285, 69
- Boselli A., Lequeux J., Gavazzi G., 2004, *A&A*, 428, 409
- Byrd G., Valtonen M., 1990, *ApJ*, 350, 89
- Chung A., van Gorkom J. H., Kenney J. D. P., Crowl H., Vollmer B., 2009, *AJ*, 138, 1741
- Cortese L., Boissier S., Boselli A., Bendo G. J., Buat V., Davies J. I., Eales S., Heinis S., Isaak K. G., Madden S. C., 2012, *A&A*, 544, A101
- Cortese L., Catinella B., Boissier S., Boselli A., Heinis S., 2011, *MNRAS*, 415, 1797
- Cortese L., Davies J. I., Pohlen M., Baes M., Bendo G. J., Bianchi S., Boselli A., 2010, *A&A*, 518, L49
- Cortese L., Gavazzi G., Boselli A., Iglesias-Paramo J., Carrasco L., 2004, *A&A*, 425, 429
- Donnelly R. H., Markevitch M., Forman W., Jones C., David L. P., Churazov E., Gilfanov M., 1998, *ApJ*, 500, 138
- Duc P.-A., Bournaud F., 2008, *ApJ*, 673, 787
- Duc P.-A., Mirabel I. F., 1994, *A&A*, 289, 83
- Fazio G. G., 2005, in Shapiro M. M., Stanek T., Wefel J. P., eds, *Neutrinos and Explosive Events in the Universe Recent Results from the Spitzer Space Telescope: A New View of the Infrared Universe*. p. 47
- Fossati M., Gavazzi G., Savorgnan G., Fumagalli M., Boselli A., Gutiérrez L., Hernández Toledo H., Giovanelli R., Haynes M. P., 2013, *A&A*, 553, A91
- Fumagalli M., Krumholz M. R., Prochaska J. X., Gavazzi G., Boselli A., 2009, *ApJ*, 697, 1811
- Gavazzi G., 1978, *A&A*, 69, 355
- Gavazzi G., Boselli A., Donati A., Franzetti P., Scodreggio M., 2003, *A&A*, 400, 451
- Gavazzi G., Boselli A., Mayer L., Iglesias-Paramo J., Vilchez J. M., Carrasco L., 2001, *ApJL*, 563, L23
- Gavazzi G., Contursi A., Carrasco L., Boselli A., Kennicutt R., Scodreggio M., Jaffe W., 1995, *A&A*, 304, 325
- Gavazzi G., Jaffe W., 1987, *A&A*, 186, L1
- Holwerda B. W., Pirzkal N., Cox T. J., de Blok W. J. G., Weniger J., Boucharad A., Blyth S.-L., van der Heyden K. J., 2011, *MNRAS*, 416, 2426
- Hota A., Saikia D. J., 2007, *Bulletin of the Astronomical Society of India*, 35, 121
- Iono D., Yun M. S., Ho P. T. P., 2005, *ApJS*, 158, 1
- Jáchym P., Combes F., Cortese L., Sun M., Kenney J. D. P., 2014, *ApJ*, 792, 11
- Kapferer W., Sluka C., Schindler S., Ferrari C., Ziegler B., 2009, *A&A*, 499, 87
- Kenney J. D. P., Geha M., Jáchym P., Crowl H. H., Dague W., Chung A., van Gorkom J., Vollmer B., 2014, *ApJ*, 780, 119
- Kenney J. D. P., van Gorkom J. H., Vollmer B., 2004, *AJ*, 127, 3361
- Koopmann R. A., Kenney J. D. P., 2004, *ApJ*, 613, 851
- Kotulla R., Fritze U., Weilbacher P., Anders P., 2009, *MNRAS*, 396, 462
- Leroy A. K., Walter F., Bigiel F., Usero A., Weiss A., Brinks E., de Blok W. J. G., Kennicutt R. C., Schuster K.-F., Kramer C., Wiesemeyer H. W., Roussel H., 2009, *AJ*, 137, 4670
- Marcolini A., Brighenti F., D'Ercole A., 2003, *MNRAS*, 345, 1329
- Meidt S. E., Schinnerer E., Knapen J. H., Bosma A., Athanassoula E., Sheth K., 2012, *ApJ*, 744, 17
- Meidt S. E., Schinnerer E., van de Ven G., Zaritsky D., Peletier R., Knapen J. H., Sheth K., Regan M., 2014, *ApJ*, 788, 144
- Mouhcine M., Kriwattanawong W., James P. A., 2011, *MNRAS*, 412, 1295
- Nishiyama K., Nakai N., Kuno N., 2001, *PASJ*, 53, 757
- Plionis M., Tovmassian H. M., Andernach H., 2009, *MNRAS*, 395, 2
- Rhoads J. E., 1998, *AJ*, 115, 472
- Roediger E., Brüggem M., 2007, *MNRAS*, 380, 1399
- Roediger E., Hensler G., 2005, *A&A*, 433, 875
- Scott T. C., Bravo-Alfaro H., Brinks E., Caretta C. A., Cortese L., Boselli A., Hardcastle M. J., Croston J. H., Plauchu I., 2010, *MNRAS*, 403, 1175
- Scott T. C., Usero A., Brinks E., Boselli A., Cortese L., Bravo-Alfaro H., 2013, *MNRAS*, 429, 221
- Sivanandam S., Rieke M. J., Rieke G. H., 2014, *ApJ*, 796, 89
- Smith R., Fellhauer M., Assmann P., 2012, *MNRAS*, 420, 1990
- Spergel D. N., Bean R., Doré O., Nolta M. R., Bennett C. L., Dunkley J., Hinshaw G., Jarosik N., Komatsu E., Page L., Peiris H. V., Verde L., Halpern M., Hill R. S., Kogut A., Limon M., Wollack E., Wright E. L., 2007, *ApJS*, 170, 377
- Steinhauser D., Haider M., Kapferer W., Schindler S., 2012, *A&A*, 544, A54
- Tonnesen S., Bryan G. L., 2009, *ApJ*, 694, 789
- Utomo D., Kriek M., Labbé I., Conroy C., Fumagalli M., 2014, *ApJL*, 783, L30
- van Gorkom J. H., 2004, in Mulchaey J. S., Dressler A., Oemler A., eds, *Clusters of Galaxies: Probes of Cosmological Structure and Galaxy Evolution Interaction of Galaxies with the Intracluster Medium*. p. 305
- Verley S., Leon S., Verdes-Montenegro L., Combes F., Sabater J., Sulentic J., Bergond G., Espada D., García E., Lisenfeld U., Odewahn S. C., 2007, *A&A*, 472, 121
- Vollmer B., Braine J., Balkowski C., Cayatte V., Duschl W. J., 2001, *A&A*, 374, 824
- Vollmer B., Braine J., Pappalardo C., Hily-Blant P., 2008, *A&A*, 491, 455
- Vollmer B., Soida M., Braine J., Abramson A., Beck R., Chung A., Crowl H. H., Kenney J. D. P., van Gorkom J. H., 2012, *A&A*, 537, A143
- Zhang H.-X., Hunter D. A., Elmegreen B. G., Gao Y., Schrub A., 2012, *AJ*, 143, 47